A&A 496, 585–595 (2009)
DOI: 10.1051/0004-6361/200811209

Astronomy & Astrophysics

Short versus long gamma-ray bursts: spectra, energetics, and luminosities

G. Ghirlanda[1], L. Nava[1,2], G. Ghisellini[1], A. Celotti[3], and C. Firmani[1,4]

[1] Osservatorio Astronomico di Brera, via E. Bianchi 46, 23807 Merate (LC), Italy
e-mail: giancarlo.ghirlanda@brera.inaf.it
[2] Università degli Studi dell'Insubria, Dipartimento di Fisica e Matematica, via Valleggio 11, 22100 Como, Italy
[3] SISSA, via Beirut 2/4, 34014, Trieste, Italy
[4] Instituto de Astronomia, Universidad Nacional Autonoma de Mexico, A.P. 70-264, 04510 Mexico D.F., Mexico

Received 22 October 2008 / Accepted 6 January 2009

ABSTRACT

We compare the spectral properties of 79 short and 79 long Gamma-Ray Bursts (GRBs) detected by BATSE and selected with the same limiting peak flux. Short GRBs have a low-energy spectral component harder and a peak energy slightly higher than long GRBs, but no difference is found when comparing short GRB spectra with those of the first 1-2 s emission of long GRBs. These results confirm earlier findings for brighter GRBs. The bolometric peak flux of short GRBs correlates with their peak energy in a similar way to long bursts. Short and long GRBs populate different regions of the bolometric fluence-peak energy plane, short bursts being less energetic by a factor similar to the ratio of their durations. If short and long GRBs had similar redshift distributions, they would have similar luminosities yet different energies, which correlate with the peak energy $E_{\rm peak}$ for the population of long GRBs. We also test whether short GRBs are consistent with the $E_{\rm peak}-E_{\rm iso}$ and $E_{\rm peak}-L_{\rm iso}$ correlations for the available sample of short (6 events) and long (92 events) GRBs with measured redshifts and $E^{\rm obs}_{\rm peak}$: while short GRBs are inconsistent with the $E_{\rm peak}-E_{\rm iso}$ correlation of long GRBs, they could follow the $E_{\rm peak}-L_{\rm iso}$ correlation of long bursts. All the above indications point to short GRBs being similar to the first phases of long bursts. This suggests that a similar central engine (except for its duration) operates in GRBs of different durations.

Key words. gamma ray: bursts – stars: neutron – radiation mechanisms: thermal

1. Introduction

Since the launch of the *Swift* satellite (Gehrels et al. 2004), several pieces of information have been added to the puzzle concerning short GRBs (e.g. see Nakar 2007; Lee & Ramirez-Ruiz 2007, for recent reviews). Short GRBs exhibit X-ray and optical afterglows, similar to those of long GRBs, and in a few cases also X-ray flares, similar to those discovered in the class of long events (e.g. Barthelmy et al. 2005). Short bursts have, on average, lower fluences and similar peak fluxes of long GRBs. Their X-ray and optical afterglows scale with the fluence (Gehrels et al. 2008; Nysewander et al. 2008). The redshift distribution of short GRBs is still an open issue due to the few secure z measured to date. Statistical studies (e.g. Magliocchetti et al. 2003; Tanvir et al. 2005; Ghirlanda et al. 2006) seem to imply that a significant fraction of the BATSE short bursts are located in the local universe, while direct z measurements, in the *Swift*-era, suggest an average $\langle z\rangle \sim 1.0$. The discovery of the intrinsically short ($T^{\rm rest}_{90} \sim 1$ s) GRB 080913 is even more challenging, being the most distant GRB to date ($z = 6.7$, Fynbo et al. 2008).

Understanding the nature of the host galaxies of short GRBs is also a challenge (e.g. Berger 2006): if they originate from a merger of two compact (evolved) objects, they should be preferentially located in early-type galaxies (although see Belczynski et al. 2008). *Swift* observations appear to infer that the formal separation at about 2 s in the (observed) duration distribution of short and long bursts might not be correct. It was known from BATSE and Hete–II (Norris & Bonnell 2006; Donaghy et al. 2006) that the short hard spikes can be followed by dim, very long-duration emission (referred to as "extended emission"). Short-spikes with extended emission were also found in the population of *Swift* GRBs (e.g. Norris & Gehrels 2008). It remains unclear whether these events represent a third category in the temporal classification of a different origin (e.g. see Zhang et al. 2007; Della Valle et al. 2006, for the case of GRB 060614).

Short GRBs have been assumed to differ from long events on the basis of their different properties in the hardness ratio-duration plot (Kouveliotou et al. 1993). However, the hardness ratio is only approximately representative of the burst spectral properties. By completing a detailed analysis of the spectra of bright BATSE short bursts, Ghirlanda et al. 2004 (GGC04 hereafter) showed that their spectra are harder than those of long GRBs, due to a harder low-energy spectral component, rather than a different peak energy. GGC04 also found that the spectra corresponding to the first 1–2 s of emission of long GRBs are similar to those of short bursts. This result relies on the detailed spectral modelling of GRB spectra rather than on the hardness-ratio analysis (but see Dong & Quin 2005; Quin & Dong 2005). Interestingly, also in the temporal domain, the properties of short GRBs appear similar to those during the first seconds of the emission of long events: Nakar & Piran (2002) found that the typical variability timescale of short GRBs (~10 ms) corresponds to that of the first 1–2 s of long ones. These results might suggest a common origin for the prompt emission of short and long GRBs.

The short burst sample analysed in GGC04 consists of the brightest 28 short GRBs detected by BATSE. It is worth exploring whether the results hold when the spectral analysis is extended to a significant number of short bursts with lower peak fluxes. In this respect, we note that for long BATSE GRBs, the

spectral properties (such as $E^{\rm obs}_{\rm peak}$, i.e., the peak energy of the νF_ν spectrum) correlate with their fluence and peak flux (Ghirlanda et al. 2008; Nava et al. 2008).

For the population of long GRBs with measured redshifts, the peak energy of the prompt emission spectrum appears to correlate with the isotropic equivalent energy $E_{\rm peak}$–$E_{\rm iso}$ (so-called "Amati" correlation, from Amati et al. 2002) and/or with the isotropic equivalent luminosity $E_{\rm peak}$–$L_{\rm iso}$ (so-called "Yonetoku" correlation, from Yonetoku et al. 2004).

The interpretation of these correlations may provide additional insight into the nature of the prompt emission. The few short GRBs with measured z and well determined spectral properties are inconsistent with the $E_{\rm peak}$–$E_{\rm iso}$ correlation (Amati 2006, 2008), but it is worth exploring whether they are consistent with the $E_{\rm peak}$–$L_{\rm iso}$ relation. It has also been shown that the rest-frame correlations ($E_{\rm peak}$–$E_{\rm iso}$ and $E_{\rm peak}$–$L_{\rm iso}$) for long GRBs correspond to observer-frame correlations between the peak energy $E^{\rm obs}_{\rm peak}$ and the fluence or peak flux (Nava et al. 2008, N08 hereafter). Therefore, there are two possible tests that can be performed: (a) compare short and long GRBs with respect to the observer frame $E^{\rm obs}_{\rm peak}$-F and $E^{\rm obs}_{\rm peak}$-P trends; (b) compare (the still few) short and long GRBs in the rest frame, where long GRBs define the $E_{\rm peak}$–$E_{\rm iso}$ and $E_{\rm peak}$–$L_{\rm iso}$ correlations.

The paper is organised as follows: in Sect. 2, we present the results of the spectral analysis of a sample of short and similarly selected/analysed long BATSE GRBs with peak flux >3 phot cm^{-2} s^{-1}; in Sect. 3, the short GRB and long BATSE GRB spectra are compared; in Sect. 4, we study the spectral-energy correlations for the population of short and long GRBs and in Sect. 5, short GRBs with known redshifts are compared with the $E_{\rm peak}$–$E_{\rm iso}$ and $E_{\rm peak}$–$L_{\rm iso}$ correlations defined by the most updated sample of long GRBs. We discuss our findings in Sect. 6.

2. Sample selection and spectral analysis

2.1. Short GRBs

GGC04 considered 28 short BATSE GRBs with peak flux exceeding $P > 10$ phot cm^{-2} s^{-1} (in the 50–300 keV energy range). To extend this analysis, we selected a sample of short duration GRBs ($T_{90\%} < 2$ s) from the BATSE on-line catalogue[1] with peak flux >3 phot cm^{-2} s^{-1} (integrated in the energy range 50–300 keV, and computed on a 64 ms timescale). In the sample of 497 triggered short BATSE events with tabulated duration, peak flux and fluence (see Magliocchetti et al. 2003), 157 short bursts satisfy the above selection criterion. This sample, used in Lazzati et al. (2005), also includes the 28 short BATSE bursts studied by GGC04.

We analysed the large area detector (LAD) spectral data of these GRBs. For 13/157 GRBs either we could not find the data (6 cases) or the data were affected by gaps (7 cases). Seventy-nine of the remaining 144 GRBs have data with a sufficient signal-to-noise (S/N) to fit the spectrum and constrain the spectral parameters, while the low S/N ratio spectrum after background subtraction for the other 65 short bursts does not allow a meaningful spectral fitting. For these 65 cases, we attempted rebinning the spectra at $>1\sigma$ to increase the signal, albeit at the expense of the spectral resolution[2]. However, for 46/65 events, the spectrum contained only one or two points after rebinning, and for 19/65, to only 5 points, not allowing us to constrain the spectral parameters of any fitted model.

[1] http://cossc.gsfc.nasa.gov/cossc/batse/

[2] The LAD spectra typically consist of 80–100 usable channels distributed in the energy range ~30 keV–1.5 MeV.

Table 1. Average properties of the selected short and long GRBs.

	$\langle T_{90}\rangle$ s	$\langle P_{50-300}\rangle$ phot cm^{-2} s^{-1}	$\langle F\rangle$ erg cm^{-2}
79 Long GRBs	17	11.5	1.7×10^{-5}
79 Short GRBs	0.73	11.12	3.6×10^{-6}

The average duration, peak flux (integrated over the 50–300 keV energy range), and fluence (for energies >25 keV) of the short and long BATSE GRBs are reported in Table 1.

The time-integrated spectrum was fitted with three spectral models typically used to analyse BATSE GRB spectra (e.g. Kaneko et al. 2006): the Band model (Band et al. 1993) consists of two smoothly joined power-law, the cutoff power-law (CPL) and single power-law model (PL). Both the CPL and the Band model exhibit a peak in their νF_ν spectrum if $\alpha > -2$ and $\beta < -2 < \alpha$, respectively, where α is the low-energy power-law photon spectral index of the CPL and Band model and β is the index of the high-energy spectral component of the latter model.

In 71/79 events, the CPL model represented a good fit to the spectra. For the remaining 8 cases, no significant curvature was found within the observed energy range and the best-fit function was given by the PL model: for these cases, only a lower or upper limit to $E^{\rm obs}_{\rm peak}$ depending on the value of the power-law index, could be set and a lower limit to bolometric fluence and peak flux (integrating over only approximately the 20–1000 keV range) could be estimated. In most cases, we could not constrain the high-energy power-law spectral index of the Band model since the typically lower flux of the high energy channels does not allow us to discriminate between a power-law component or an exponential cutoff, in most fits the CPL model was statistically more robust than the Band one simply because it has one parameter less. As already discussed in GGC04, we could not perform a time-resolved spectral analysis with the LAD data of short BATSE bursts: if and how their spectrum evolve during the burst duration remains an open issue.

The results of the spectral analysis of the time integrated-spectra of the 79 short GRBs are reported in Table 6 ordered for decreasing peak flux (Col. 3, as reported in the BATSE on-line catalogue). The spectral parameters of the best-fit function (CPL or PL model) are listed in Cols. 4–6. In the final two columns, we report the bolometric (1–10 000 keV) fluence and flux estimated from the best-fit model parameters. When only a lower or upper limit on the energy E_0 could be determined the fluences and peak energy fluxes are computed in the observed energy range 20–1000 keV.

2.2. Long GRBs

To compare the spectral properties of short and long GRBs, we considered long BATSE bursts selected with the same criterion as for the short ones. We note that the available samples of BATSE bursts with spectral information (e.g. Preece et al. 2000; Kaneko et al. 2006) were selected with different criteria: in particular, an analysis by Kaneko et al. (2006) examined bursts selected according to either peak flux or fluence as part of the aim of performing time-resolved spectral analysis with a minimum number of spectra distributed within each burst.

For this reason, we randomly extracted from the data set of 400 long BATSE GRBs with peak flux >3 ph cm^{-2} s^{-1} a representative sub-sample of 79 GRBs by requiring that they followed the Log N–Log P defined by the entire sample of long BATSE bursts.

In this case we also excluded events with S/N ratio insufficient to constrain properly the spectral parameters. We performed both the time-integrated and time-resolved spectral analysis, adopting the models defined in Sect. 2. In 34/79 cases, the time-integrated spectrum is well described by a CPL spectral shape. However, for 44/79 GRBs the spectrum shows a high energy power-law tail and the Band model provides a more reliable fit than the CPL one. Only in one case is the best fit model function a simple power-law.

The time-integrated spectral results of the 79 long GRBs are reported in Table 7. The bolometric fluence (Col. 8) and peak flux (Col. 9) are both estimated by integrating the best-fit model in the 1 keV–10 MeV energy range. For one GRBs (trigger 6400) the spectrum is well fitted by a simple power-law. In this case we estimated only a lower limit on fluence and peak flux.

3. Short versus long: spectra

3.1. Time integrated spectra

The distribution of short and long BATSE bursts in the hardness ratio-duration plane (e.g. Kouveliotou et al. 1993) implies that long and short GRBs are two separate classes with short GRBs being on average harder than long ones. However, similarly to long GRBs, the spectrum of short GRBs presents a significant curvature in the BATSE spectral range. GGC04 compared the low-energy power-law index α and the peak energy $E^{\rm obs}_{\rm peak}$ of 28 bright ($P \geq 10$ ph cm^{-2} s^{-1}) short bursts with those of long bursts selected on the basis of a similar limiting peak-flux (Ghirlanda et al. 2002). Despite the small sample, their results suggest that a statistically significant difference existed in the low-energy part of the spectrum, such that short bursts had a harder spectral index α: the average values being $\langle\alpha_{\rm short}\rangle = -0.58 \pm 0.10$ and $\langle\alpha_{\rm long}\rangle = -1.05 \pm 0.14$ (K–S probability $P_{\rm KS} \sim 0.04\%$). The peak energy $E^{\rm obs}_{\rm peak}$ of long bursts ($\langle E^{\rm obs}_{\rm peak}\rangle = 520 \pm 90$ keV) is only slightly higher than that of short events ($\langle E^{\rm obs}_{\rm peak}\rangle = 355 \pm 30$ keV) with $P_{\rm KS} \sim 0.8\%$.

We test these results using the larger samples of short and long GRBs considered here, which extend the sample of GGC04 to the 3 ph cm^{-2} s^{-1} peak flux threshold. The distributions of α and $E^{\rm obs}_{\rm peak}$ for the time-integrated spectra of the 79 short and long bursts are shown in Fig. 1. They can be modelled well by Gaussian functions: the best-fit model parameters (μ and σ, representing the mean value and the standard deviation) are reported in Table 2. The K–S test probability that the distributions were drawn from the same parent one are reported in Table 3. For long events we report in Table 3 three cases: spectral parameters derived from the spectrum of 1) the whole emission, 2) the first second and 3) the first two seconds of emission. For both α and $E^{\rm obs}_{\rm peak}$ the probabilities increase considering only the very first phases of long bursts.

The low-energy spectral index of short bursts is harder than that of long GRBs $\langle\alpha_{\rm short}\rangle = -0.4 \pm 0.5$ and $\langle\alpha_{\rm long}\rangle = -0.92 \pm 0.42$ ($P_{\rm KS} = 8.8$e–5), while their peak-energy distributions are more similar ($P_{\rm KS} = 1.3\%$). This result confirms (see GGC04) that the spectral difference between short and long GRBs as observed in the hardness-duration plane, is due to a harder low-energy spectrum of short bursts rather than a significantly different peak energy.

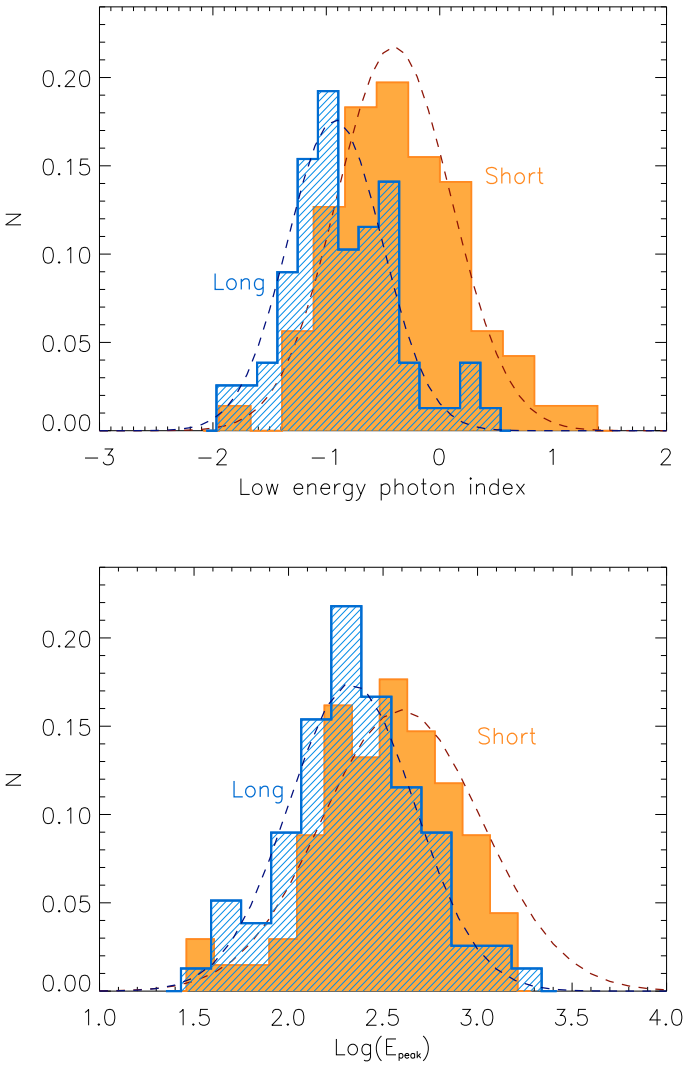

Fig. 1. Spectral parameter distributions normalised to the total number. *Top*: low energy photon spectral index (α) for the 79 short (filled histogram) and the 79 long (hatched histogram) GRBs analysed in this work. The dashed lines represent the Gaussian fit to these distributions. *Bottom*: peak energy of the νF_ν spectrum ($E^{\rm obs}_{\rm peak}$) for the two samples).

3.2. Time resolved spectra of long bursts

GGC04 found some evidence that the spectrum of short GRBs is similar (in terms of α and $E^{\rm obs}_{\rm peak}$) to the spectrum of the first 1–2 s of the long events (the K–S probability of 83% for α and 10% for $E^{\rm obs}_{\rm peak}$). This result is intriguingly in agreement with the findings that the variability timescale of short GRBs resembles that of the first 1–2 s of long events (Nakar & Piran 2002).

With the larger, uniformly analysed, samples of short and long GRBs examined here, we can meaningfully compare the time-resolved spectra of long GRBs during the first 2 s of emission and the time-integrated spectra of short ones. In Fig. 2, we report the α and $E^{\rm obs}_{\rm peak}$ distributions of the 79 short bursts with those determined by the time-resolved spectral analysis of long bursts within one and two seconds of the trigger: the

Table 2. Parameters of the Gaussian fits of the distributions of the spectral parameters of short and long GRBs.

	α				$E_{\rm peak}$			
	Short	Long	Long 1 s	Long 2 s	Short	Long	Long 1 s	Long 2 s
μ	–0.40	–0.92	–0.65	–0.63	2.60	2.33	2.49	2.48
σ	0.50	0.42	0.50	0.45	0.42	0.33	0.35	0.36

Table 3. K–S test probability that the distributions of short and long GRB spectral parameters are drawn from the same parent population.

	Long	Long 1 s	Long 2 s
α	8.8e-7	0.0433	0.00457
$E_{\rm peak}$	0.013	0.965	0.764

corresponding K–S probabilities (see Table 3) indicate that they are very similar. The difference found between the time-integrated spectra of short and long bursts could be due simply to a hard-to-soft evolution of the spectrum of long GRBs, which become on average softer with time than that of short bursts. While this should be tested by comparing the spectral evolution of short and long GRBs, as already found in GGC04 and mentioned above, the low S/N of the data used here prevents us from performing a time-resolved spectral analysis for the short BATSE bursts.

4. Short versus long GRBs: observer-frame correlations

Long bursts follow some empirical correlations involving the (isotropic) energetics $E_{\rm iso}$ (Amati et al. 2002) and/or peak luminosity $L_{\rm iso}$ (Yonetoku et al. 2004), and the rest-frame peak energy $E_{\rm peak}$. N08 demonstrated that correlations also hold between the observed peak energy $E^{\rm obs}_{\rm peak}$ and the fluence (F) or observed peak flux (P). This opens the possibility of examining the impact of instrumental selection effects on these correlations: in particular, both the trigger threshold, i.e. the minimum peak flux required to trigger a given detector, and the "spectral analysis" threshold, i.e. the minimum signal for a spectrum to be analysed, are functions of $E^{\rm obs}_{\rm peak}$. However, as N08 emphasized, the correlation between peak energy and peak flux in the observer frame of BATSE long GRBs is not induced by these thresholds.

In comparing the distributions of the (observed) $E^{\rm obs}_{\rm peak}$-fluence and $E^{\rm obs}_{\rm peak}$-peak flux for our representative sample of 79 short and long GRBs, we computed the bolometric (1–10 000 keV) fluence and peak flux by integrating the best-fit CPL or Band model. When the best fit model was instead a simple power-law, we can only estimate a lower limit to the fluence (or peak flux) by integrating the spectrum over the range 20–1000 keV and an upper/lower limit to $E^{\rm obs}_{\rm peak}$, depending on the value of the fitted power-law index.

4.1. E^{obs}_{peak} versus peak flux

The 79 short and long GRBs populate similar regions of the $E^{\rm obs}_{\rm peak}$-P observer-frame plane[3] (Fig. 3). For comparison in the figure, we also report the complete sample of long GRBs (with fluence $>2\times10^{-6}$ erg cm^{-2}) analysed in N08 (filled circles) and the (incomplete) samples of long bursts detected by instruments other than BATSE (open circles). The dotted line represents the trigger threshold of BATSE (adapted from Band 2006 – see N08 for details).

To understand the impact of the selection threshold of the sample (photon peak-flux >3 phot cm^{-2} s^{-1} between 50 and 300 keV) on the distribution of bursts in the $E^{\rm obs}_{\rm peak}$–P plane, we transformed the limiting photon-flux in bolometric energy-flux

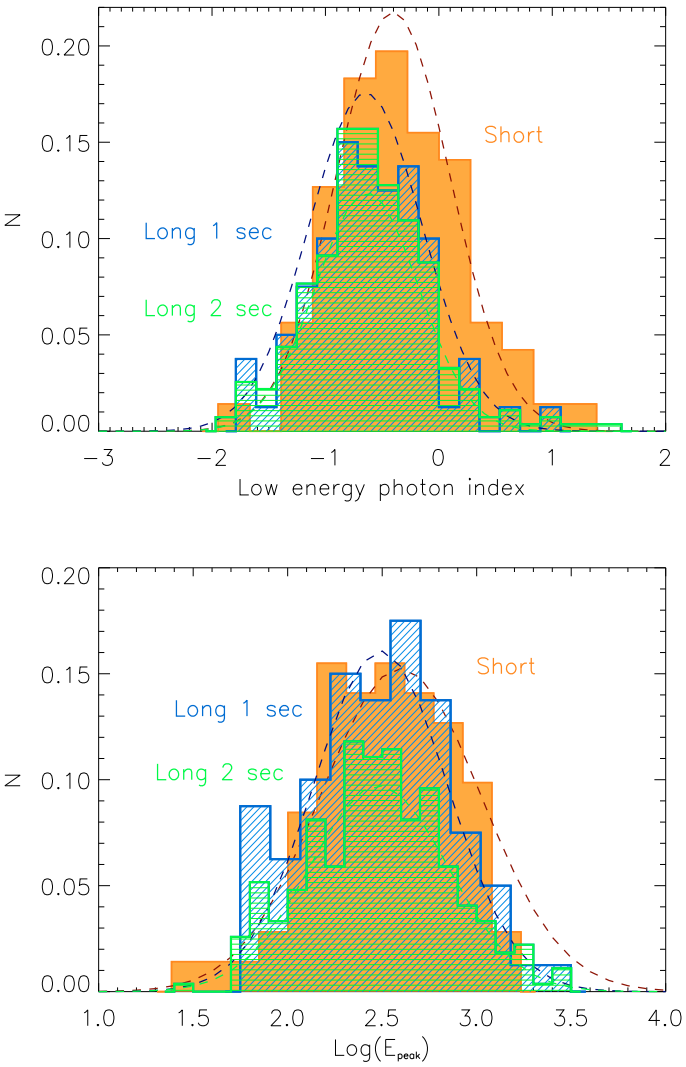

Fig. 2. Spectral parameter distributions normalised to the total number of spectra. *Top*: low energy photon spectral index α for the 79 short GRBs (filled histogram) and for the time resolved spectra of the first second (hatched oblique histogram) and the first two seconds (hatched horizontal histogram) of long bursts. The dashed lines represent the Gaussian fit to the distributions. *Bottom*: peak energy of the νF_ν spectrum for the same population of short and long bursts.

[3] P is the bolometric peak flux in erg cm^{-2} s^{-1}.

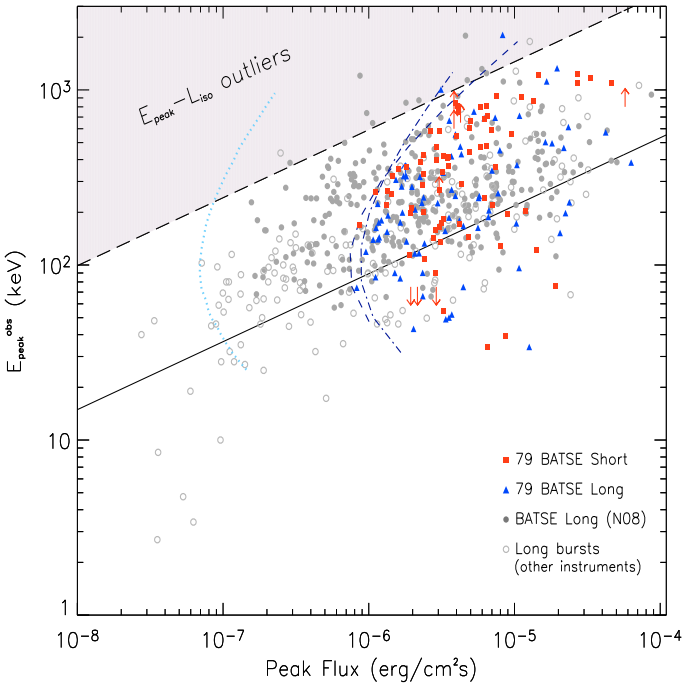

Fig. 3. Distribution in the E^{obs}_{peak}–P plane of the 79 long (triangles) and 79 short (squares) bursts considered here. Arrows correspond to upper/lower limits to E^{obs}_{peak}, and in these cases the estimated P is a lower limit. For comparison also the BATSE bursts from Kaneko et al. (2006) and N08 (filled circles) and the bursts detected by instruments other than BATSE (empty circles – see N08) are reported. The dotted line represents the trigger threshold for BATSE GRBs, i.e. the minimum peak flux needed to trigger the instrument. The dot-dashed and dashed lines are the P limit criterion adopted to select the 79 long and 79 short GRBs, respectively: namely a photon peak flux of 3 phot cm^{-2} s^{-1} (in the energy range 50–300 keV) and a typical spectrum with $\alpha \simeq -0.5$ and $\alpha \simeq -1.0$ for short and long GRBs, respectively. The solid line indicates the E_{peak}–L_{iso} correlation (as derived with the most updated sample of 92 GRBs with known z in Sect. 5) transformed in the observer frame E^{obs}_{peak}–P plane. The shaded region corresponds to a "region of outliers", namely values of E^{obs}_{peak} and P inconsistent (at more than 3σ) with the E_{peak}–L_{iso} correlation for any GRB redshift.

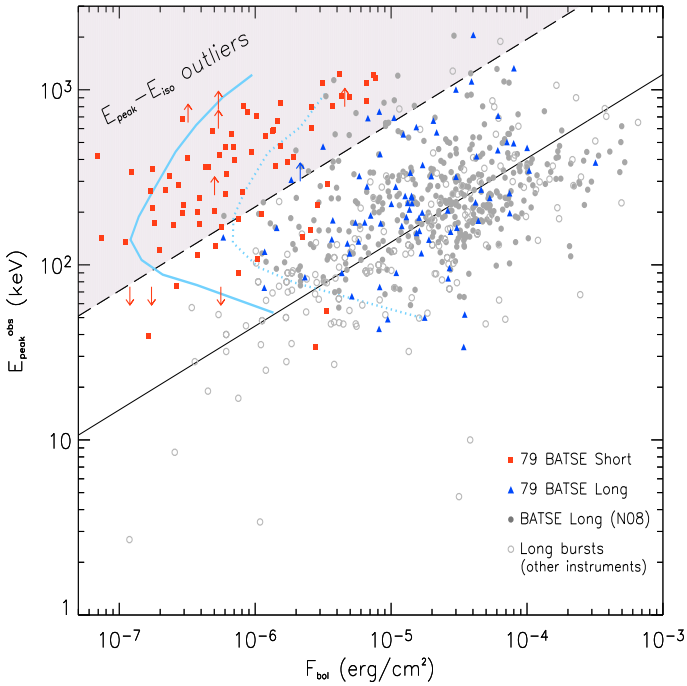

Fig. 4. Distribution of bursts in the E^{obs}_{peak}–F plane. Squares (triangles) represent the sample of 79 short (long) bursts discussed in Sect. 2. The dotted and solid curves show the spectral threshold, i.e. the minimum fluence as a function of E^{obs}_{peak} necessary to perform a reliable spectral analysis and constrain the value of E^{obs}_{peak} itself. The threshold depends on the burst duration and on the spectral shape (see Ghirlanda et al. 2008, for more details): the dotted curve is estimated for long bursts while the solid curve is derived for a typical short burst of 0.7 s duration and $\alpha = -0.5$ (as found in Sect. 2). The solid line indicates the E_{peak}–E_{iso} correlation (as derived with the most updated sample of 92 GRBs with known z in Sect. 5) transformed in the observer frame E^{obs}_{peak}–F plane. The shaded region represents the "region of outliers", namely values of E^{obs}_{peak} and F inconsistent (at more than 3σ) with the E_{peak}–E_{iso} correlation for any redshift.

by simulating different spectra with a variable E^{obs}_{peak} and fixed typical values of α ($\alpha \simeq -1$ and $\simeq -0.5$ for long and short bursts, respectively), normalised to the photon peak flux. The corresponding curves (dot-dashed and dashed lines for long and short GRBs, respectively) are shown in Fig. 3: the BATSE trigger threshold is more than a factor of 10 lower than the imposed selection criterion.

While the 79 long bursts confirm the existence of an E^{obs}_{peak}-P correlation independent of the instrumental effect due to the trigger threshold (see N08), for short bursts the analysed range of peak flux is insufficient to draw a definitive conclusion. The selection cut at low peak fluxes strongly affects the short-burst sample in the E^{obs}_{peak}-P plane. However, it is interesting to note that both short and long GRBs – selected with the same criterion – are consistent with the correlation defined by larger samples of long events, which suggests the possibility that short bursts also follow the same (or a similar) E^{obs}_{peak}-P correlation exhibited by long events.

In the E^{obs}_{peak}–P plane, we can also test the possible consistency of short GRBs with the E_{peak}–L_{iso} correlation, namely $E_{peak} \propto L^{0.4}_{iso}$. This correlation is updated and presented for short and long GRBs in the next section, but restricted to GRBs with known redshifts. Assigning different redshifts to a GRB of unknown z, we define a trajectory in the rest-frame E_{peak}–L_{iso} plane. This curve can intersect the E_{peak}–L_{iso} correlation or become consistent with its 3σ scatter. If not, the considered GRB is an outlier. Correspondingly, we can define the "outlier" region in the observer E^{obs}_{peak}–P plane (see Nakar & Piran 2005; Ghirlanda et al. 2005; N08). This is the region where a GRB, regardless of redshift, is inconsistent with the E_{peak}–L_{iso} correlation, within its 3σ scatter. The shaded region in Fig. 3 represent this region: no short burst of the 79 analysed is an outlier of the E_{peak}–L_{iso} correlation.

4.2. E^{obs}_{peak} versus fluence

An analysis similar to that presented above can be performed by considering the bolometric fluence. If the GRB redshift is known, from the bolometric fluence one can derive the isotropic equivalent energy, which was found to be correlated with the rest-frame peak energy (Amati et al. 2002; Amati 2006).

In Fig. 4, the 79 short and long BATSE bursts (squares and triangles, respectively) are reported together with the sample of

Table 4. Long GRBs with measured redshifts and spectral parameters not already in the sample of 83 bursts considered by N08. References: (1) Golenetskii et al. (2008a); (2) Ohno et al. (2008); (3) Barthelmy et al. (2008); (4) Tueller et al. (2008); (5) Golenetskii et al. (2008a), GCN 7854; (6) Golenetskii et al. (2008b); (7) Golenetskii et al. (2008c); (8) Meegan et al. (2008a); (9) Baumgartner et al. (2008).

GRB	z	α	Peak flux	Range (keV)	$L_{\rm iso}$ 10^{52} erg/s	$E_{\rm peak}$ (keV)	Fluence (10^{-6})	Range keV	$E_{\rm iso}$ 10^{52} erg	Ref.
080411	1.03	–1.51(0.05)	1.3(0.2)e-5	20–2000	9.4(0.4)	526(63)	63(3.1)	20–2000	24(2)	1
080413	2.433	–1.2(0.1)	0.8(0.2)	15–1000	0.6(0.1)	584(206)	4.8(1.0)	15–1000	8.5(1.0)	2
080413B	1.1	–1.26(0.27)	18.7(0.8)	15–150	1.7(0.3)	154(33)	3.2(0.1)	15–150	2.0(0.4)	3
080603B	2.69	–1.21(0.3)	1.5(0.4)e-6	20–1000	12(0.5)	376(76)	2.4(0.1)	20–1000	11(1.6)	4
080605	1.639	–1.03(0.07)	1.6(0.3)e-5	20–2000	32(1.3)	252(19)	30.2(1.2)	20–2000	25.3(3.6)	5
080607	3.036	–1.08(0.07)	2.7(0.5)e-5	20–4000	217(10)	1691(170)	89(5)	20–4000	200(13)	6
080721[a]	2.591	–0.9(0.1)	2.0(0.3)e-5	20–5000	102(15)	1742(226)	84(6)	20–5000	120(12)	7
080810	3.35	–0.91(0.12)	1.9(0.2)	50–300	9.3(0.9)	1488(348)	6.9(0.5)	50–300	39(3.7)	8
080916A	0.689	–1.17(0.21)	2.7(0.2)	15–150	0.08(0.02)	161(39)	4.0(0.1)	15–150	1(0.2)	9

[a] Band spectrum with $\beta = -2.43 \pm 0.35$.

Table 5. Short GRBs with measured redshifts and spectral parameters. References: (1) Villasenor et al. (2005); (2) Golenetskii et al. (2005); (3) Golenetskii et al. (2006); (4) Ohno et al. (2007); (5) Golenetskii et al. (2007); (6) Pal'Shin et al. (2008).

GRB	z	α	Peak flux	Range (keV)	$L_{\rm iso}$ 10^{52} erg/s	$E_{\rm peak}$ (keV)	Fluence (10^{-6})	Range keV	$E_{\rm iso}$ 10^{52} erg	Ref.
050709	0.16	–0.53(0.12)	5.1(0.5)e-6	2–400	0.05(0.01)	97.4(11.6)	0.4(0.04)	2–400	0.0033(0.0001)	1
051221	0.5465	–1.08(0.13)	4.6(1.3)e-5	20–2000	6.42(0.56)	620(186)	3.2(0.9)	20–2000	0.3(0.04)	2
061006	0.4377	–0.62(0.2)	2.1e-5	20–2000	1.78(0.23)	955(267)	3.57	20–2000	0.2(0.03)	3
070714	0.92	–0.86(0.1)	2.8(0.3)	100–1000	1.4(0.1)	2150(1113)	3.7	15–2000	1.1(0.1)	4
071020	2.145	–0.65(0.3)	6.0e-6	20–2000	22(1)	1013(205)	7.7	20–2000	10.2(1.5)	5
080913	6.7	–0.89(0.52)	1.4(0.2)	15–1000	11.4(1.5)	1009(200)	0.9	15–1000	7.14(0.9)	6

long BATSE GRBs (filled circles) analysed by N08. In contrast to our results for the $E^{\rm obs}_{\rm peak}$–P plane, short and long bursts occupy different regions of the $E^{\rm obs}_{\rm peak}$–F plane, having similar $E^{\rm obs}_{\rm peak}$ but fluences scaling by a factor comparable to the ratio of their durations. As discussed by Ghirlanda et al. (2008), the observer frame $E^{\rm obs}_{\rm peak}$–F plane is biased mostly by the "spectral analysis" threshold, which corresponds to a requirement on the S/N in order to constrain the spectral parameters. The solid curve represents the "spectral threshold" which is estimated for short bursts as described by Ghirlanda et al. (2008): we adopted the typical value of $\alpha = -0.5$ determined in Sect. 3 and the representative duration of the short bursts included in our sample, namely $T_{90} \sim 0.7$ s. A burst with $E^{\rm obs}_{\rm peak}$ and F values so that it is located to the right of this curve has sufficient signal to allow a reliable spectral analysis. The dotted curve in the figure represents the "spectral threshold" for the population of long GRBs (see N08 for the relevance of this selection effect to the properties of long GRBs in the $E^{\rm obs}_{\rm peak}$–F plane).

Figure 4 reveals that the spectral threshold affects the distribution of short bursts significantly. This was expected since out of 144 bursts that satisfy the peak flux selection criterion and with available data only for 79 the spectral parameters could be constrained. Due to these limitations, no conclusion can be inferred about any true (i.e. not determined by selection effects) $E^{\rm obs}_{\rm peak}$–F correlation for short bursts. However, it is clear from Fig. 4 that short and long GRBs are highly scattered in the $E^{\rm obs}_{\rm peak}$–F plane and that short GRBs do not follow the same correlation defined by long events.

Finally, in the $E^{\rm obs}_{\rm peak}$–F plane, we can test the consistency of short GRBs with the $E_{\rm peak}$–$E_{\rm iso}$ correlation defined by long events (see Sect. 5). The region containing outliers is populated significantly: the majority of short GRBs (∼78%) are inconsistent with the $E_{\rm peak}$–$E_{\rm iso}$ correlation defined by long bursts.

5. Short versus long GRBs: energetics and luminosities

The comparison between the data for short and long GRBs in the observer frame planes has shown that although short and long bursts have similar peak fluxes and peak energies, and can follow the same correlation in the $E^{\rm obs}_{\rm peak}$–P plane, the distributions of long and short GRBs are inconsistent in the $E^{\rm obs}_{\rm peak}$–F plane because of the lower fluence of short GRBs.

In this section, we examine the isotropic energy and luminosity of the two populations and consider in particular the two correlations, i.e. $E_{\rm peak}$–$E_{\rm iso}$ and $E_{\rm peak}$–$L_{\rm iso}$, with similar slopes and different normalisations, defined by long GRBs with measured z.

Amati (2006) considered two short bursts with robust redshift and peak energy determinations that are inconsistent with the $E_{\rm peak}$-$E_{\rm iso}$ correlation defined by long GRBs: these two events are 3 orders of magnitude less energetic than long GRBs of similar peak energy. A similar conclusion was reached by Amati (2008) for a sample of 5 short GRBs.

However, the results presented in Sect. 4 indicate that short and long GRBs have comparable properties in the $E^{\rm obs}_{\rm peak}$–P plane, and that none of the 79 short events without a redshift is a clear outlier of the $E_{\rm peak}$–$L_{\rm iso}$ correlation: this is consistent with the hypothesis that both populations follow the same (rest-frame) $E_{\rm peak}$–$L_{\rm iso}$ correlation of long GRBs. The different region

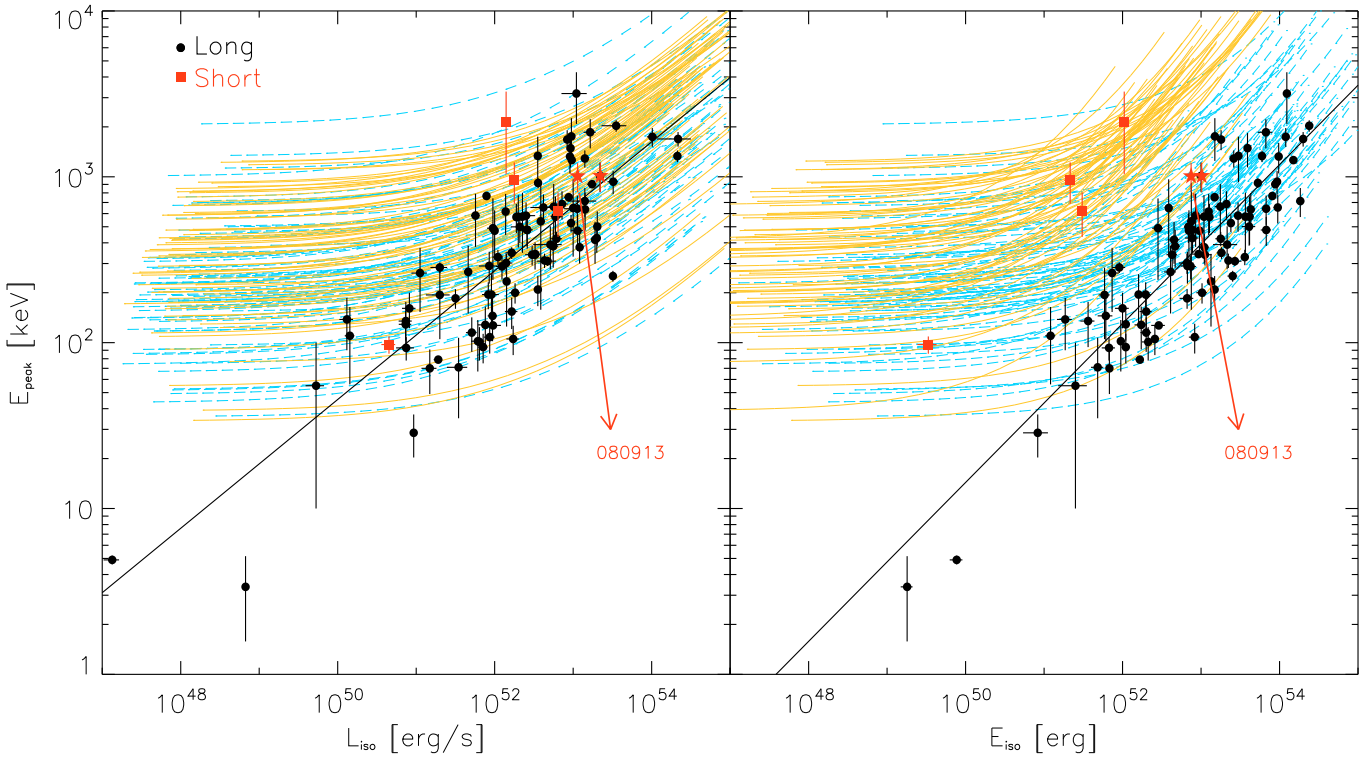

Fig. 5. Rest-frame peak energy versus isotropic luminosity (*left*) and isotropic energy (*right*) for 92 long (filled circles) and 6 short (filled squares and stars) GRBs with measured redshifts. The solid lines represent the best fit of the correlation defined by long GRBs: $E_{\rm peak} \propto L_{\rm iso}^{0.4}$ and $E_{\rm peak} \propto E_{\rm iso}^{0.5}$. The 1σ scatter is 0.23 dex and 0.27 dex for the $E_{\rm peak}-L_{\rm iso}$ and $E_{\rm peak}-E_{\rm iso}$ correlation, respectively. The orange and blue (dashed) lines indicate where the 79 short and long GRBs would be located for different redshifts (between 0.1 and 10). GRB 080913 (at $z = 6.7$) and GRB 071020 (at $z = 2.145$) are considered short events (filled stars) even though their observed duration is $\simeq$8 and $\simeq$4 s, respectively.

occupied by short and long bursts in the $E_{\rm peak}^{\rm obs}$–F plane might also indicate that their rest-frame properties differ.

We test these possibilities for the available sample (updated to contain bursts until Sept. 2008) of short and long GRBs with measured peak energy and redshift. The long GRB sample consists of the 83 GRBs considered by N08, which was updated by adding the 9 long GRBs detected from March to September 2008 (Table 4). Similarly, we searched the literature for data of all the short GRBs with measured z and spectral properties. There are a dozen GRBs with measured redshifts that are defined in the literature as short events based on their duration. In this class, there are few bursts composed by a short spike followed by long-lasting ("extended") emission (e.g., GRB 050724, GRB 061006, and GRB 070714B, but see also Zhang et al. 2007, for the case of 060614). The short-duration, hard, initial spike has properties similar to those of short GRBs without the extended emission (Norris & Gehrels 2008). Among the short GRBs with extended emission, we consider only the two cases (GRB 061006 and GRB 070714B) in which the short spike spectrum has a measured $E_{\rm peak}^{\rm obs}$. In addition to these, there are 2 short GRBs, without extended emission, which have both z and $E_{\rm peak}^{\rm obs}$ measured. These are GRB 050709 and GRB 051221.

In the sample of short GRBs (reported in Table 5) we also include the detected GRB 080913 ($z = 6.7$), which would be classified as a long event based on its observed duration (~8 s), but it is intrinsically short. This seems to be supported by the hardness of this event (Perez-Ramirez et al. 2008, but see Greiner et al. 2008). A similar case is GRB 071020, which is at relatively high redshift ($z = 2.145$, Jakobsson et al. 2007) but has an intrinsic duration that implies it is a member of the short class.

In Fig. 5, we show the sample of 92 long GRBs (solid filled circles), which define the $E_{\rm peak}-L_{\rm iso}$ and $E_{\rm peak}-E_{\rm iso}$ correlation (left and right panels in Fig. 5, respectively). The solid (black) lines in Fig. 5 are the best-fit functions to the correlations for the sample of long GRBs:

$$E_{\rm peak} \propto L_{\rm iso}^{0.4} (\sigma = 0.27) \quad (1)$$

$$E_{\rm peak} \propto E_{\rm iso}^{0.5} (\sigma = 0.23), \quad (2)$$

where σ is the standard deviation of the scatter of the data points perpendicular to the best-fit model relations. Short GRBs (filled squares) are inconsistent with the $E_{\rm peak}-E_{\rm iso}$ correlation (right panel in Fig. 5), while they are consistent with the $E_{\rm peak}-L_{\rm iso}$ one, defined by long GRBs (left panel in Fig. 5).

For the 79 short and long GRBs analyzed in this paper, we do not know the redshift. However, we can test their consistency with the correlations of Fig. 5 by assigning a redshift z between 0.1 and 10. For each burst and for each redshift, we therefore compute the rest-frame peak energy $E_{\rm peak} = (1+z)E_{\rm peak}^{\rm obs}$, the bolometric isotropic energy $E_{\rm iso} = 4\pi {\rm d}_L(z)^2 F/(1+z)$, and the bolometric isotropic luminosity $L_{\rm iso} = 4\pi {\rm d}_L(z)^2 P$ (where ${\rm d}_L(z)$ is the luminosity distance).

The curves in Fig. 5 indicate where the 79 short (shaded curves) and long GRBs (solid curves) move in the $E_{\rm peak}-L_{\rm iso}$ and $E_{\rm peak}-E_{\rm iso}$ planes (left and right panels of Fig. 5, respectively) if they are assigned a redshift between 0.1 and 10. As a support of the tests on outliers presented in Figs. 3 and 4, data

Table 6. The sample of 79 short BATSE GRBs.

Trig.	T_{90} s	P phot/(cm^2 s)	α	E_0 keV	χ^2(d.o.f.)	Fluence erg/cm^2	Peak flux erg/(cm^{2}s)
6293	0.192 ± 0.091	88.53 ± 1.00	−1.27 ± 0.02		1.216(109)	4.56E-6	>5.74E-5
298	0.455 ± 0.065	56.13 ± 1.27	−0.57 ± 0.92	85.38 ± 64.90	1.113(102)	1.99E-7	1.43E-5
3412	0.068 ± 0.006	54.82 ± 0.76	−1.31 ± 0.52	110.20 ± 80.98	0.892(103)	2.62E-7	1.91E-5
6668	0.116 ± 0.006	39.12 ± 0.61	−0.39 ± 0.49	126.80 ± 62.57	1.184(107)	4.99E-7	1.18E-5
444	0.256 ± 0.091	28.55 ± 0.76	−0.87 ± 0.23	113.50 ± 28.39	1.132(102)	5.07E-7	8.04E-6
2514	0.200 ± 0.094	28.40 ± 0.74	−0.81 ± 0.14	163.30 ± 25.95	1.129(100)	1.12E-6	8.99E-6
3152	1.793 ± 0.066	25.34 ± 0.72	−0.40 ± 0.09	683.70 ± 116.50	1.175(107)	6.55E-6	4.64E-5
5561	0.104 ± 0.011	19.28 ± 0.45	−1.20 ± 1.48	48.51 ± 25.00	0.956(108)	1.65E-7	8.69E-6
3087	1.152 ± 0.091	18.68 ± 0.58	−1.19 ± 0.15	273.10 ± 74.50	1.103(76)	2.89E-6	7.02E-6
2273	0.224 ± 0.066	18.59 ± 0.55	−0.18 ± 0.45	132.70 ± 49.46	0.886(100)	3.88E-7	6.26E-6
7281	1.664 ± 0.143	16.83 ± 0.42	−0.83 ± 0.15	123.30 ± 18.60	1.296(107)	2.21E-6	4.80E-6
2068	0.591 ± 0.060	15.63 ± 0.59	−0.22 ± 0.26	97.07 ± 22.85	1.210(107)	3.91E-7	4.19E-6
2125	0.223 ± 0.013	15.42 ± 0.56	−0.48 ± 0.30	240.50 ± 90.00	0.844(102)	4.57E-7	7.43E-6
3173	0.208 ± 0.025	14.90 ± 0.58	−1.00 ± 0.18	559.60 ± 281.65	1.356(105)	6.69E-7	9.52E-6
2679	0.256 ± 0.091	13.73 ± 0.51	−0.32 ± 0.13	650.20 ± 149.25	1.363(107)	3.14E-6	2.72E-5
1553	0.960 ± 0.143	13.70 ± 0.52	−0.87 ± 0.11	764.00 ± 183.60	1.173(96)	6.62E-6	1.35E-5
6123	0.186 ± 0.042	12.83 ± 0.42	−0.23 ± 1.64	76.66 ± 49.00	1.107(108)	1.11E-7	3.10E-6
6635	1.152 ± 0.143	12.05 ± 0.39	−1.74 ± 0.15	129.50 ± 32.70	1.014(91)	2.76E-6	6.57E-6
1088	0.192 ± 0.091	11.92 ± 0.55	0.10 ± 2.11	68.08 ± 61.79	1.186(104)	7.41E-8	2.80E-6
1453	0.192 ± 0.453	11.89 ± 0.51	−0.16 ± 0.65	94.20 ± 48.00	0.812(108)	1.80E-7	3.17E-6
6535	1.664 ± 0.143	11.88 ± 0.38	−0.97 ± 0.08	1175.60 ± 384.27	1.391(108)	7.36E-6	1.47E-5
2320	0.608 ± 0.041	11.03 ± 0.47	−0.58 ± 0.19	129.00 ± 26.10	0.794(103)	7.57E-7	3.23E-6
2933	0.320 ± 0.091	10.77 ± 0.44	0.22 ± 0.62	130.20 ± 55.94	1.429(107)	3.42E-6	4.33E-6
7939	1.039 ± 0.072	10.77 ± 0.38	−0.41 ± 0.15	99.73 ± 12.96	1.193(82)	2.53E-6	2.86E-6
2614	0.296 ± 0.057	10.49 ± 0.52	−1.00 ± 0.18	469.60 ± 222.80	0.836(108)	6.08E-7	5.84E-6
2715	0.384 ± 0.091	10.47 ± 0.50	0.08 ± 0.11	562.80 ± 85.20	1.049(108)	7.69E-6	3.30E-5
2896	0.456 ± 0.033	10.44 ± 0.48	−0.87 ± 0.26	79.94 ± 18.19	1.072(106)	7.53E-7	2.89E-6
7784	1.918 ± 1.995	10.29 ± 0.34	−0.83 ± 0.35	140.20 ± 54.30	1.432(108)	5.63E-7	3.05E-6
2317	0.896 ± 0.091	9.73 ± 0.46	−0.53 ± 0.25	73.46 ± 13.12	1.249(65)	1.04E-6	2.41E-6
2834	0.680 ± 0.011	8.79 ± 0.44	−0.54 ± 0.24	407.60 ± 168.80	1.165(85)	1.36E-6	6.90E-6
6679	1.408 ± 0.091	8.62 ± 0.35	−0.61 ± 0.27	318.90 ± 141.60	1.409(107)	9.39E-7	4.91E-6
6527	1.856 ± 0.516	8.47 ± 0.38	−1.32 ± 0.21	80.36 ± 15.60	1.090(95)	3.33E-6	3.25E-6
7353	0.249 ± 0.004	8.47 ± 0.38	0.00 ± 0.22	615.80 ± 197.40	1.181(107)	4.19E-6	2.72E-5
5277	0.496 ± 0.023	8.14 ± 0.33	0.29 ± 0.24	208.40 ± 30.81	0.885(106)	1.54E-6	6.46E-6
8104	0.384 ± 0.091	8.13 ± 0.30	0.42 ± 1.35	110.60 ± 70.37	0.774(107)	2.20E-7	3.04E-6
2330	0.804 ± 0.009	8.03 ± 0.39	−0.86 ± 0.29	616.90 ± 491.30	0.961(75)	1.02E-6	6.54E-6
6263	1.984 ± 0.181	7.99 ± 0.31	−0.36 ± 0.64	69.14 ± 30.59	1.054(107)	3.78E-7	1.91E-6
5339	0.832 ± 0.091	7.77 ± 0.33	−0.40 ± 0.10	567.90 ± 99.64	0.732(93)	4.95E-6	1.12E-5
603	1.472 ± 0.272	7.50 ± 0.56	−0.71 ± 0.63	155.30 ± 93.62	1.004(85)	3.78E-7	2.36E-6
6368	0.896 ± 0.326	7.24 ± 0.34	−1.37 ± 0.18		0.997(108)	3.21E-7	>4.26E-6
6606	0.704 ± 0.389	7.16 ± 0.29	−1.77 ± 0.20		0.973(108)	5.02E-7	>3.04E-6
3642	0.704 ± 0.091	6.83 ± 0.31	0.21 ± 0.88	89.97 ± 58.42	1.262(107)	2.92E-7	1.93E-6
6671	0.256 ± 0.091	6.71 ± 0.31	−1.39 ± 0.13		0.937(100)	5.36E-7	>3.84E-6
5647	1.088 ± 0.326	6.50 ± 0.32	−0.06 ± 0.80	108.50 ± 115.16	1.366(107)	1.74E-7	1.95E-6
7375	0.311 ± 0.073	6.40 ± 0.31	−0.47 ± 0.87	267.90 ± 200.05	1.039(101)	3.19E-7	3.46E-6
677	0.055 ± 0.008	6.21 ± 0.44	0.65 ± 1.29	127.20 ± 168.26	0.751(105)	1.22E-7	3.18E-6
1076	0.161 ± 0.016	6.18 ± 0.44	−2.46 ± 0.33		1.417(89)	1.20E-7	>2.16E-6
936	1.438 ± 0.065	5.85 ± 0.44	−0.84 ± 0.26	341.50 ± 179.45	1.069(104)	7.03E-7	2.91E-6
5607	1.088 ± 0.091	5.85 ± 0.30	−0.71 ± 0.23	426.20 ± 199.45	1.150(82)	1.19E-6	3.97E-6
7142	0.969 ± 0.064	5.81 ± 0.28	0.94 ± 0.33	124.10 ± 12.79	0.953(107)	1.42E-6	3.50E-6
4955	0.464 ± 0.036	5.73 ± 0.31	−1.04 ± 0.45	298.20 ± 371.80	1.176(107)	2.71E-7	2.33E-6
4776	0.448 ± 0.091	5.54 ± 0.28	−0.19 ± 0.32	232.70 ± 88.45	1.152(107)	6.90E-8	3.27E-6
7813	0.564 ± 0.164	5.37 ± 0.29	−2.68 ± 0.17		1.053(108)	5.59E-7	>1.94E-6
1760	0.576 ± 0.143	5.27 ± 0.35	−0.25 ± 0.28	188.70 ± 56.95	1.027(105)	6.18E-7	2.37E-6
7378	1.247 ± 0.077	5.25 ± 0.33	−0.52 ± 0.16	536.20 ± 153.35	1.465(107)	2.60E-6	5.87E-6
4660	1.168 ± 0.080	5.15 ± 0.29	0.56 ± 0.21	161.70 ± 23.80	0.919(87)	1.92E-6	3.53E-6
5533	0.768 ± 0.091	5.12 ± 0.30	0.02 ± 0.15	335.20 ± 60.15	0.971(87)	2.91E-7	6.26E-6
7078	0.448 ± 0.091	5.11 ± 0.42	−3.60 ± 0.45		0.920(108)	1.73E-7	>2.90E-6
5527	0.820 ± 0.008	5.04 ± 0.26	−0.34 ± 0.11	489.30 ± 88.30	0.760(90)	3.73E-6	6.41E-6
3735	1.301 ± 0.091	4.83 ± 0.29	0.00 ± 0.18	301.70 ± 55.05	1.286(107)	2.60E-6	4.91E-6
3297	0.272 ± 0.023	4.45 ± 0.33	−0.83 ± 0.37	496.80 ± 501.70	1.198(106)	4.90E-7	3.07E-6
2952	0.680 ± 0.018	4.37 ± 0.34	−0.69 ± 0.25	570.20 ± 312.15	0.791(107)	8.76E-7	4.13E-6
5599	0.598 ± 0.043	4.24 ± 0.26	−0.79 ± 0.30	664.70 ± 637.40	1.234(106)	8.25E-7	4.07E-6
5529	1.015 ± 0.129	4.23 ± 0.29	1.37 ± 0.96	65.65 ± 22.09	1.015(106)	2.95E-7	1.31E-6
7133	1.079 ± 0.37	4.08 ± 0.26	−0.14 ± 0.29	135.80 ± 36.25	1.115(107)	6.01E-7	1.43E-6

Table 6. continued.

Trig.	T_{90} s	P phot/(cm^2 s)	α	E_0 keV	χ^2(d.o.f.)	Fluence erg/cm^2	Peak flux erg/(cm^{2}s)
7793	1.093 ± 0.04	3.99 ± 0.27	−0.05 ± 0.22	470.90 ± 126.35	1.054(106)	4.34E-6	7.56E-6
2377	0.496 ± 0.011	3.98 ± 0.33	0.06 ± 0.26	229.30 ± 55.10	0.875(100)	6.90E-7	2.91E-6
3606	1.824 ± 0.066	3.95 ± 0.26	0.19 ± 0.35	175.90 ± 49.60	1.216(102)	1.72E-6	2.26E-6
3113	0.976 ± 0.023	3.90 ± 0.35	−0.78 ± 0.16	690.00 ± 316.25	1.145(90)	1.54E-6	3.95E-6
6715	0.452 ± 0.027	3.71 ± 0.26	−0.25 ± 0.78	206.20 ± 187.77	1.178(107)	4.34E-7	1.83E-6
575	0.413 ± 0.022	3.70 ± 0.46	0.17 ± 0.87	121.40 ± 63.56	0.890(106)	1.71E-7	1.35E-6
2217	0.656 ± 0.029	3.56 ± 0.31	0.36 ± 0.27	281.00 ± 93.35	1.234(73)	1.46E-6	4.97E-6
3921	0.464 ± 0.161	3.52 ± 0.24	0.36 ± 0.48	179.90 ± 66.60	1.086(106)	5.42E-7	2.39E-6
5206	0.304 ± 0.023	3.46 ± 0.28	−1.23 ± 0.09		1.219(107)	3.81E-7	>2.34E-6
2918	0.448 ± 0.091	3.44 ± 0.34	−0.60 ± 0.63	252.50 ± 195.90	1.085(100)	1.77E-7	1.59E-6
3940	0.576 ± 0.091	3.19 ± 0.22	−0.33 ± 0.44	101.80 ± 40.67	1.187(97)	2.50E-7	8.64E-7
7912	1.856 ± 0.707	3.10 ± 0.25	−0.28 ± 0.26	150.90 ± 47.65	1.236(107)	8.05E-7	1.11E-6
6341	1.920 ± 0.707	3.05 ± 0.28	−0.25 ± 0.29	332.00 ± 143.20	0.878(107)	1.34E-6	2.64E-6
3359	0.344 ± 0.025	3.01 ± 0.25	0.67 ± 0.90	121.00 ± 74.79	1.037(104)	2.35E-7	1.46E-6

for short GRBs in Fig. 5 (left) are consistent with the $E_{\rm peak}$–$L_{\rm iso}$ correlation defined by long events (filled circles), while most are inconsistent with the $E_{\rm peak}$–$E_{\rm iso}$ correlation (right) defined by long bursts (filled circles).

We note that in the $E_{\rm peak}$–$E_{\rm iso}$ plane, short GRBs at $z < 1.0$ are outliers whereas the two high-redshift events GRBs (GRB 071020 at $z = 2.145$, and GRB 080913 at $z = 6.7$) are consistent within the 3σ scatter of the $E_{\rm peak}$–$E_{\rm iso}$ correlation.

6. Summary and conclusions

We have presented a spectral analysis of of 79 short GRBs detected by BATSE with peak flux >3 phot cm^{-2} s^{-1} (integrated in the 50–300 keV energy range). These data were compared with those of a representative sample of 79 long BATSE GRBs with the same flux limit. For both short and long GRBs, we have analysed the time-integrated spectra with the typical models adopted (see e.g. Kaneko et al. 2006); a time-resolved spectral analysis has also been performed for long events.

Most of the short GRB spectra were reproduced more accurately by a cutoff power-law model. For the population of long GRBs, 56% of the spectra are fitted by a Band and the 43% by a cutoff power-law model. This might reflect a genuine intrinsic difference between the spectra of short and long GRBs or could be due to observational selection effects. The low S/N of the high-energy part of the BATSE spectrum does not allow us to exclude that, as for long events, short bursts also have a high-energy spectral tail. The BGO detectors of the GBM experiment onboard Fermi/GLAST (Meegan et al. 2008b) extend the spectral range of the NaI detectors (similar to the BATSE LAD) to a few tenths of MeV: this will allow us to test the nature of short GRB high-energy emission.

The comparison of the spectral properties of short and long GRBs shows that:

– The time-averaged spectrum of short GRBs is harder than that of long GRBs due to a harder low-energy spectral component. The peak energy distribution is, instead, only slightly offset towards higher energy for short than for long bursts. Therefore, the difference observed in the hardness-duration plane between the two populations is due to the different distribution of α (Fig. 1);

– The spectrum of short GRBs is similar to the spectrum of the first 1–2 s of emission of long GRBs (Fig. 2), both in terms of the low-energy spectral index and the peak energy. This is intriguingly consistent with the similar variability of short and the first few seconds of emission from long bursts (Nakar & Piran 2002) and might indicate that a common mechanism operates during the first few seconds after the trigger for all events.

We compared the distribution of short and long GRBs in the observer frame $E^{\rm obs}_{\rm peak}$-Peak flux and $E^{\rm obs}_{\rm peak}$-Fluence planes, where long GRBs are known to follow well defined correlations (Ghirlanda et al. 2008, Nava et al. 2008):

– Short GRBs have a similar $E^{\rm obs}_{\rm peak}$ and peak flux of long GRBs and, indeed, populate the same region in the $E^{\rm obs}_{\rm peak}$-Peak flux plane, although short bursts tend to occupy the high peak flux-peak energy range of the correlation defined by long GRBs (Fig. 3). This suggests that short events can be consistent with the rest-frame $E_{\rm peak}$–$L_{\rm iso}$ correlation defined by long GRBs, if their redshift distribution is similar (as also supported by the redshift distribution of the few short GRBs known to date).
– Short GRBs, instead, have fluences lower than those of long events, and are inconsistent with the empirical correlation defined by long GRBs in the $E^{\rm obs}_{\rm peak}$-Fluence plane (Fig. 4). This implies that the majority of short GRBs (78%) are outliers of the $E_{\rm peak}$–$E_{\rm iso}$ correlation defined by long bursts.

Finally, we compared the intrinsic properties of short and long GRBs with known redshift (Fig. 5). Although only a few short bursts have measured z and well determined spectral properties, we find that while short GRBs are inconsistent with the $E_{\rm peak}$–$E_{\rm iso}$ correlation defined by long GRBs, they are consistent with the $E_{\rm peak}$–$L_{\rm iso}$ correlation of the 92 GRBs with available z (updated to contain data to Sept. 2008).

We conclude that the comparison of the characteristics of short GRB with those of the first seconds of emission of long GRBs indicate that the two population show (i) the same variability (Nakar & Piran 2002); (ii) the same spectrum; (iii) the same luminosity; and (iv) are consistent with the same $E_{\rm peak}$–$L_{\rm iso}$ correlation. All of these similarities strongly suggest a common (or similar) dissipation process – and possibly central

Table 7. The sample of 79 long BATSE GRBs.

Trig.	T_{90} s	P phot/(cm^2 s)	α	β	E_0 keV	χ^2(d.o.f.)	Fluence erg/cm^2	Peak flux erg/(cm^{2}s)
160	17.024	4.21	−0.44 ± 0.07		112.16 ± 7.16	1.006(69)	5.47E-6	1.1707E-6
543	4.8640	11.158	−0.87 ± 0.05	−2.42 ± 0.10	219.22 ± 18.01	0.870(82)	1.27E-5	5.7328E-6
907	158.08	3.744	0.07 ± 0.09	−2.87 ± 0.16	92.76 ± 6.49	1.245(68)	7.07E-6	1.3548E-6
973	89.984	5.707	−1.03 ± 0.04	−2.15 ± 0.04	278.59 ± 22.03	1.132(98)	4.59E-5	3.7020E-6
1122	18.752	13.787	−0.91 ± 0.04	−2.54 ± 0.05	149.82 ± 7.85	0.955(85)	3.05E-5	5.6131E-6
1157	170.56	12.187	−1.01 ± 0.05	−2.23 ± 0.06	206.93 ± 19.32	0.855(90)	2.61E-5	6.6804E-6
1159	18.240	3.727	−0.81 ± 0.09		257.21 ± 36.81	0.708(58)	1.84E-6	1.5362E-6
1425	10.432	9.52	−1.52 ± 0.03		346.21 ± 26.32	0.992(76)	1.20E-5	4.4592E-6
1625	16.128	28.061	−0.82 ± 0.01	−2.43 ± 0.06	393.90 ± 14.21	1.202(103)	1.00E-4	2.1800E-5
1886	275.71	16.683	−0.43 ± 0.02	−2.25 ± 0.05	315.04 ± 11.47	1.208(103)	7.97E-5	1.8097E-5
1922	16.192	3.532	−1.03 ± 0.13		168.01 ± 31.15	0.691(48)	1.44E-6	1.1215E-6
2037	6.2720	8.355	−1.03 ± 0.05		709.27 ± 117.6	0.924(78)	6.75E-6	6.1974E-6
2067	30.848	18.919	−0.52 ± 0.01	−3.15 ± 0.07	173.18 ± 2.77	1.177(97)	7.44E-5	7.7100E-6
2083	15.168	46.554	−1.17 ± 0.02	−2.41 ± 0.03	238.88 ± 9.69	3.283(96)	7.47E-5	2.2391E-5
2367	18.816	4.6	0.45 ± 0.18		92.73 ± 13.21	0.762(36)	5.83E-7	1.1793E-6
2393	5.1340	4.388	−1.29 ± 0.27	−2.86 ± 0.06	61.29 ± 16.24	0.841(53)	8.16E-6	2.0287E-6
2446	8.2560	4.378	−0.64 ± 0.05		207.11 ± 14.64	1.067(73)	6.65E-6	1.6800E-6
2537	4.8000	27.283	−1.38 ± 0.04	−2.89 ± 0.07	154.85 ± 10.03	1.078(75)	2.69E-5	1.0752E-5
2611	12.212	35.05	−1.07 ± 0.02		662.87 ± 46.27	1.666(88)	1.53E-5	2.3439E-5
2793	6.9760	5.086	−0.53 ± 0.05		509.84 ± 46.32	0.820(86)	8.19E-6	5.2682E-6
2890	51.584	3.008	−0.98 ± 0.04		988.18 ± 118.43	1.033(103)	3.00E-5	3.1272E-6
2913	22.912	5.738	−1.31 ± 0.14		168.67 ± 36.05	0.961(56)	4.95E-6	2.0695E-6
2958	36.896	3.939	−0.95 ± 0.11		133.66 ± 15.29	0.948(53)	3.66E-6	1.1608E-6
2993	44.800	4.255	−1.00 ± 0.03		2065.78 ± 298.74	0.938(102)	4.02E-5	8.2881E-6
2994	48.576	15.349	−1.03 ± 0.01		1374.62 ± 93.16	0.958(100)	8.01E-5	1.9596E-5
3039	3.6350	9.048	−0.70 ± 0.06		102.33 ± 5.49	1.298(61)	4.77E-6	2.4114E-6
3110	10.176	4.449	−0.05 ± 0.06		285.55 ± 19.04	0.962(90)	1.23E-5	3.9332E-6
3138	5.1840	16.833	−1.32 ± 0.03		277.05 ± 17.82	1.515(75)	1.30E-5	6.6159E-6
3178	39.936	14.583	−1.09 ± 0.01		782.28 ± 35.70	1.638(103)	6.13E-5	1.0825E-5
3255	34.880	12.667	−1.89 ± 0.04		325.08 ± 39.89	1.334(77)	3.42E-5	1.2624E-5
3269	13.888	8.365	−0.66 ± 0.04		516.69 ± 48.49	1.091(89)	1.05E-5	7.3692E-6
3287	33.408	7.714	−1.19 ± 0.11		281.28 ± 56.33	0.924(74)	1.43E-5	2.9709E-6
3306	108.51	3.496	−1.13 ± 0.41	−2.28 ± 0.12	96.75 ± 56.07	0.617(78)	2.63E-5	1.6435E-6
3352	46.336	3.84	−0.81 ± 0.05	−2.84 ± 0.15	129.93 ± 8.327	0.965(75)	2.74E-5	1.3351E-6
3436	40.000	3.89	−1.09 ± 0.09	−2.26 ± 0.17	227.08 ± 43.66	0.875(80)	1.37E-5	2.0817E-6
3648	57.088	5.907	−1.08 ± 0.11	−2.65 ± 0.13	126.45 ± 18.19	0.955(67)	1.67E-5	2.2141E-6
3776	11.072	5.897	−0.46 ± 0.07		113.65 ± 7.41	0.927(64)	6.40E-6	1.6459E-6
3905	24.256	4.675	−1.21 ± 0.06		352.68 ± 53.12	1.313(79)	1.08E-5	1.9777E-6
4048	13.696	4.864	−0.51 ± 0.08	−2.41 ± 0.15	225.22 ± 26.67	0.843(83)	1.38E-5	3.2398E-6
4350	52.000	3.521	−1.92 ± 0.07		642.17 ± 227.12	0.957(76)	1.77E-5	3.5523E-6
4710	9.9840	3.012	−0.25 ± 0.95	−2.12 ± 0.08	51.53 ± 36.96	1.036(57)	4.34E-6	1.5089E-6
5526	72.448	3.779	−1.34 ± 0.05		490.21 ± 93.28	1.168(82)	1.98E-5	1.8081E-6
5530	4.9550	6.695	−1.19 ± 0.11		82.07 ± 7.92	1.260(46)	5.14E-6	2.3486E-6
5563	4.8900	22.704	−1.01 ± 0.08	−2.41 ± 0.09	175.29 ± 23.56	1.191(72)	8.38E-6	1.0300E-5
5601	19.456	4.9375	−0.56 ± 0.09	−2.52 ± 0.18	157.04 ± 18.81	1.207(77)	1.32E-5	2.3136E-6
5628	15.872	8.9689	−1.35 ± 0.03		384.96 ± 33.81	0.975(78)	1.42E-5	3.9267E-6
5704	10.048	43.927	−1.52 ± 0.06		320.81 ± 56.10	0.741(73)	1.54E-5	2.0545E-5
5711	2.2400	41.245	−1.04 ± 0.03	−2.04 ± 0.09	599.11 ± 69.74	1.069(95)	2.16E-5	4.2236E-5
5773	31.488	15.209	−0.28 ± 0.02		103.86 ± 1.49	2.148(80)	4.38E-5	4.1832E-6
5955	11.648	3.5974	−0.76 ± 0.22		95.97 ± 19.25	0.921(38)	1.17E-6	9.5567E-7
6100	16.256	19.4123	−0.98 ± 0.02	−2.27 ± 0.08	491.21 ± 27.50	1.228(107)	7.12E-5	1.6291E-5
6235	4.0320	21.7417	−0.74 ± 0.03		294.73 ± 14.46	1.092(90)	1.71E-5	1.0389E-5
6251	3.0080	7.5941	−1.05 ± 0.10		497.31 ± 128.32	1.018(61)	3.16E-6	4.2470E-6
6266	37.568	4.0372	−0.61 ± 0.04	−2.63 ± 0.20	229.27 ± 16.52	1.035(90)	3.00E-5	2.2454E-6
6336	6.5280	15.6576	−1.08 ± 0.02		1214.97 ± 88.84	0.964(101)	3.91E-5	1.6621E-5
6400	14.080	4.0832	−1.72 ± 0.05			0.907(53)	2.15E-5	>1.7827E-6
6422	6.5920	8.2515	−1.27 ± 0.11	−3.44 ± 0.14	66.92 ± 6.48	1.944(55)	9.46E-6	3.3758E-6
6546	6.7840	3.3192	−0.45 ± 0.29		47.65 ± 7.69	0.500(32)	1.17E-6	8.2697E-7
6560	36.800	11.8054	−0.67 ± 0.04		143.28 ± 6.96	1.279(73)	1.61E-5	3.5545E-6
6593	31.232	10.1204	−0.93 ± 0.03	−2.28 ± 0.07	225.64 ± 15.44	1.236(96)	5.32E-5	5.6690E-6
6814	19.264	3.5187	−0.31 ± 0.38	−2.15 ± 0.09	80.42 ± 26.71	1.002(59)	5.76E-6	1.8153E-6
6816	35.136	5.5426	−1.68 ± 0.09		499.27 ± 166.46	1.093(63)	1.62E-5	3.3415E-6
6930	36.800	5.7627	−0.62 ± 0.25	−2.34 ± 0.08	65.41 ± 15.49	0.924(66)	1.09E-5	2.3424E-6
7185	147.45	5.8478	−1.66 ± 0.12		153.26 ± 30.25	1.295(40)	3.48E-5	3.7113E-6
7255	10.304	5.391	−0.61 ± 0.05	−2.73 ± 0.18	174.32 ± 13.16	1.117(82)	1.42E-5	2.3779E-6

Table 7. continued

Trig.	T_{90} s	P phot/(cm^2 s)	α	β	E_0 keV	χ^2(d.o.f.)	Fluence erg/cm^2	Peak flux erg/(cm^{2}s)
7318	14.976	4.0609	-0.58 ± 0.03		469.06 ± 30.66	1.053(93)	2.05E-5	3.5686E-6
7329	3.1360	4.2126	0.36 ± 0.09	-2.59 ± 0.24	181.90 ± 16.54	0.964(81)	8.29E-6	4.3176E-6
7374	12.160	4.6678	0.32 ± 0.10		77.58 ± 4.71	0.626(61)	3.73E-6	1.2204E-6
7429	17.856	3.6964	0.22 ± 0.07		100.66 ± 4.95	1.057(70)	1.01E-5	1.1517E-6
7464	41.088	5.797	-0.78 ± 0.03	-2.73 ± 0.22	342.83 ± 19.63	1.188(97)	4.26E-5	3.6946E-6
7515	328.44	3.2372	-0.47 ± 0.10	-2.28 ± 0.11	130.60 ± 16.54	1.111(78)	1.69E-5	1.7024E-6
7518	12.736	3.7771	0.26 ± 0.18		142.20 ± 19.32	0.670(74)	5.84E-6	1.7344E-6
7678	42.752	11.7202	-0.81 ± 0.03	-2.53 ± 0.09	290.72 ± 14.39	1.473(107)	1.04E-4	7.0047E-6
7906	15.168	91.4818	-1.09 ± 0.01	-2.27 ± 0.02	420.65 ± 11.75	2.032(107)	3.19E-4	6.3174E-5
7932	67.392	3.1139	-1.23 ± 0.08		181.15 ± 21.32	1.712(78)	1.90E-5	1.0716E-6
7954	15.040	56.9544	-0.93 ± 0.02	-2.80 ± 0.12	212.67 ± 8.64	1.529(95)	4.18E-5	2.3804E-5
7998	10.240	4.505	-0.53 ± 0.19		57.98 ± 7.61	1.016(36)	2.32E-6	1.1128E-6
8008	22.656	9.0618	-0.46 ± 0.03	-2.42 ± 0.09	293.21 ± 14.55	1.285(97)	6.10E-5	7.9296E-6
8099	15.488	8.5515	-1.59 ± 0.07		181.37 ± 21.05	1.460(55)	8.25E-6	4.4529E-6

engine – acting in both classes of GRBs. In this respect the only difference could be the engine lifetime.

These results do not necessarily require a similar progenitor. Both the core collapse of a massive star and the merging of two compact objects can produce a black hole accreting material from a dense disc/torus. In this respect, one of the major differences between the two scenarios is the absence of a supernova event accompanying short GRBs, as confirmed by the observations. The other expected difference is in the redshift distribution of the two populations (but see e.g. Belczynski et al. 2008), although the detection of GRB 080913 (at $z = 6.7$) challenges this possibility.

Acknowledgements. We thank M. Nardini, D. Burlon and F. Tavecchio for useful discussions. We acknowledge ASI (I/088/06/0), a 2007 PRIN–INAF grant and the MIUR for financial support. C. Halliday is acknowledged for language editing. This research has made use of the data obtained through the High Energy Astrophysics Science Archive Research Center Online Service, provided by the NASA/Goddard Space Flight Center.

References

Amati, L. 2006, MNRAS, 372, 233
Amati, L. 2008, Relativistic Astrophysics: 4th Italian-Sino Workshop, AIP, 966, 3
Amati, L., Frontera, F., Tavani, M., et al. 2002, A&A, 390, 81
Band, D. 2006, ApJ, 644, 378
Band, D., Matteson, J., Ford, L., et al. 1993, ApJ, 413, 281
Barthelmy, S. D., Chincarini, G., Burrows, D. N., et al. 2005, Nature, 438, 994
Barthelmy, S. D., Baumgartner, W., & Cummings, J. 2008, GCN, 7606
Baumgartner, W., Barthelmy, S. D., & Cummings, J. 2008, GCN, 8243
Belczynski, K., Kalogera, V., Rasio, F. A., et al. 2008, ApJS, 174, 223
Berger, E. 2006, Gamma-Ray Bursts in the Swift Era, Conf. Proc., AIP, 836, 33
Della Valle, M., Chincarini, G., Panagia, N., et al. 2006, Nature, 444, 1050
Donaghy, T. Q., Lamb, D. Q., Sakamoto, T., et al. 2006 [arXiv:astro-ph/0605570]
Dong, Y.-M., & Qin, Y.-P. 2005, MNRAS, 358, 1267
Fynbo, J. P. U., Greiner, J., & Kruehler, T. 2008, GCN, 8225
Gehrels, N., Chincarini, G., Giommi, P., et al. 2004, ApJ, 661, 1005
Gehrels, N., Barthelmy, S. D., Burrows, D. N., et al. 2008, ApJ, in press [arXiv:0808.3391]
Ghirlanda, G., Celotti, A., & Ghisellini, G. 2002, A&A, 393, 409
Ghirlanda, G., Ghisellini, G., & Celotti, A. 2004, A&A, 422, L55 (GGC04)
Ghirlanda, G., Ghisellini, G., & Firmani, C. 2005, MNRAS, 361, L10
Ghirlanda, G., Magliocchetti, M., Ghisellini, G., & Guzzo, L. 2006, MNRAS, 368, L20
Ghirlanda, G., Nava, L., Ghisellini, G., Firmani, C., & Cabrera, J. I. 2008, MNRAS, 387, 319
Golenetskii, S., Aptekar, R., Mazets, E., et al. 2005, GCN, 4394
Golenetskii, S., Aptekar, R., Mazets, E., et al. 2006, GCN, 5710
Golenetskii, S., Aptekar, R., Mazets, E., et al. 2007, GCN, 6960
Golenetskii, S., Aptekar, R., Mazets, E., et al. 2008a, GCN, 7589
Golenetskii, S., Aptekar, R., Mazets, E., et al. 2008b, GCN, 7854
Golenetskii, S., Aptekar, R., Mazets, E., et al. 2008c, GCN, 7995
Greiner, J., Kruhler, T., Fynbo, J. P. U., et al. 2008, ApJ, subm. [arXiv:0810.2314]
Jakobsson, Vreeswijk, P. M., Hjorth, J., et al. 2007, GCN, 6952
Kaneko, Y., Preece, R. D., Briggs, M. S., et al. 2006, ApJS, 166, 298
Kouveliotou, C., Meegan, C. A., Fishman, G. J., et al. 1993, ApJ, 413, L101
Lazzati, D., Ghirlanda, G., & Ghisellini, G. 2005, MNRAS, 362, L8
Lee, W. H., & Ramirez-Ruiz, E. 2007, NJPh, 9, 17
Magliocchetti, M., Ghirlanda, G., & Celotti, A. 2003, MNRAS, 343, 255
Meegan, C. A., Greiner, J., & Bhat, N. P. 2008a, GCN, 8100
Meegan, C., Bhat, N., & Bissaldi, E. 2008b, GAMMA-RAY BURSTS 2007: Proceedings of the Santa Fe Conference, AIP, 1000, 573
Nakar, E. 2007, PhR, 442, 166
Nakar, E., & Piran, T. 2002, MNRAS, 330, 920
Nakar, E., & Piran, T. 2005, MNRAS, 360, L73
Nava, L., Ghirlanda, G., Ghisellini, G., & Firmani, C. 2008, MNRAS, in press [arXiv:0807.4931]
Norris, J. P., & Bonnell, J. T. 2006, ApJ, 643, 266
Norris, J. P., & Gehrels, N. 2008, Proceedings of the Santa Fe Conference, AIP Conf. Proc., 1000, 280
Nysewander, M., Fruchter, A. S., & Pe'er, A. 2008, ApJ, subm. [arXiv:0806.3607]
Ohno, M., Uehara, T., Takahashi, T., et al. 2007, GCN, 6638
Ohno, M., Kokubun, M., Suzuki, M., Takahashi, T., et al. 2008, GCN, 7630
Pal'Shin, V., Golenetskii, S., Aptekar, R., et al. 2008, GCN, 8256
Perez-Ramirez, D., de Ugarte-Postigo, A., Gorosabel, M. A., et al. 2008, A&A, subm. [arXiv:0810.2107]
Preece, R. D., Briggs, M. S., & Mallozzi, R. S. 2000, ApJS, 126, 19
Quin, Y.-P., & Dong, Y.-M. 2005, MNRAS, 358, 1320
Tanvir, N. R., Chapman, R., Levan, A. J., & Priddey, R. S. 2005, Nature, 438, 991
Tueller, J., Barthelmy, S. D., Baumgartner, W., et al. 2008
Zhang, B. 2007, ChJAA, 7, 1
Yonetoku, D., Murakami, T., Nakamura, T., et al. 2004, ApJ, 609, 935
Villasenor, J. S., Lamb, D. Q., Ricker, G. R., et al. 2005, Nature, 437, 855